nature structural & molecular biology

Mediator Head module structure and functional interactions

Gang Cai[1], Tsuyoshi Imasaki[2], Kentaro Yamada[2], Francesco Cardelli[2], Yuichiro Takagi[2] & Francisco J Asturias[1]

We used single-particle electron microscopy to characterize the structure and subunit organization of the Mediator Head module that controls Mediator–RNA polymerase II (RNAPII) and Mediator-promoter interactions. The Head module adopts several conformations differing in the position of a movable jaw formed by the Med18–Med20 subcomplex. We also characterized, by structural, biochemical and genetic means, the interactions of the Head module with TATA-binding protein (TBP) and RNAPII subunits Rpb4 and Rpb7. TBP binds near the Med18–Med20 attachment point and stabilizes an open conformation of the Head module. Rpb4 and Rpb7 bind between the Head jaws, establishing contacts essential for yeast-cell viability. These results, and consideration of the structure of the Mediator–RNAPII holoenzyme, shed light on the stabilization of the pre-initiation complex by Mediator and suggest how Mediator might influence initiation by modulating polymerase conformation and interaction with promoter DNA.

Transcriptional regulation is focused on the initiation process, which entails recruitment of RNAPII and the general transcription factors to a promoter. Both basal and activated transcription are critically dependent on the Mediator complex[1–5], which conveys regulatory signals to RNAPII. Consistent with its essential role, the Mediator complex is conserved in sequence and structure throughout the eukaryotes[6–8]. Unfortunately, despite the paramount importance of Mediator, the mechanism of action of the complex remains unclear, highlighting the significance of investigating its structure, subunit organization and conformational variability.

Biochemical and structural analyses have shown that Mediator has a modular organization. Biochemically defined subunit modules appear to correspond to structural modules identified by structural studies. Recent cryo–electron microscopy (EM) analysis of Mediator (**Fig. 1a**) identified rigid portions of the Mediator structure that undergo conserved large-scale rearrangements, which appear to be essential for the interaction of Mediator with RNAPII and other components of the basal transcription machinery[8].

Of all Mediator modules, the Head is perhaps the most critical, as evidenced by cessation of mRNA synthesis at nearly all promoters *in vivo* when Head module function is compromised in a Med17 temperature-sensitive *Saccharomyces cerevisiae* mutant strain[9–11]. Consistent with this observation, all but two (Med18 and Med20) Head module subunits are essential for cell viability. The Head module is involved in at least two critical steps in the regulation of transcription initiation. First, chromatin immunoprecipitation analysis of *GAL4* promoter activation in *S. cerevisiae* showed that the Head module is required for promoter recognition *in vivo*: compromised Head module function in the Med17 temperature-sensitive mutant results in impaired Mediator recruitment to the promoter[11]. Second, the Head module is involved in the assembly and/or stabilization of the transcription pre-initiation complex (PIC), most likely through direct interactions with RNAPII and additional components of the basal transcription machinery[8,11].

To understand how the Head module might carry out these essential functions, it is critical to characterize the module's structure and possible conformational rearrangements so as to understand how Head module subunits are organized and how the Head module interacts with PIC components to enable regulation of transcription initiation. Here we present the results from single-particle EM, biochemical, genetic and functional analyses of recombinant Head and Head subcomplexes that define the subunit organization of the module; these analyses reveal a dynamic conformation that appears to be influenced by interaction with the TATA-binding protein (TBP). We also document the significance of essential contacts between the Head module and the Rpb4–Rpb7 RNAPII subunit complex, and we consider possible implications for the mechanism of initiation regulation by Mediator.

RESULTS

Recombinant Head module and its subcomplexes

A previously established robust expression system provided access to Mini, Core and full Mediator Head module assemblies and made possible biochemical and structural studies[11]. However, a drawback of this system was that it required repeated rounds of screening to identify individual recombinant baculoviruses that would result in high levels of expression of Mediator subunits. To overcome this problem, we prepared single baculoviruses bearing all genes encoding the subunits of the full Mediator Head module (Med17, Med6, Med18, Med8, Med20, Med11 and Med22) and of the Core (Med17, Med6, Med8, Med11 and Med22) and Mini (Med17, Med11 and Med22) subcomplexes using the MultiBac system[12]. We recovered the three

[1]Department of Cell Biology, The Scripps Research Institute, La Jolla, California, USA. [2]Department of Biochemistry and Molecular Biology, Indiana University School of Medicine, Indianapolis, Indiana, USA. Correspondence should be addressed to F.J.A. (asturias@scripps.edu) or Y.T. (ytakagi@iupui.edu).

Received 13 May 2009; accepted 3 December 2009; published online 14 February 2010; doi:10.1038/nsmb.1757

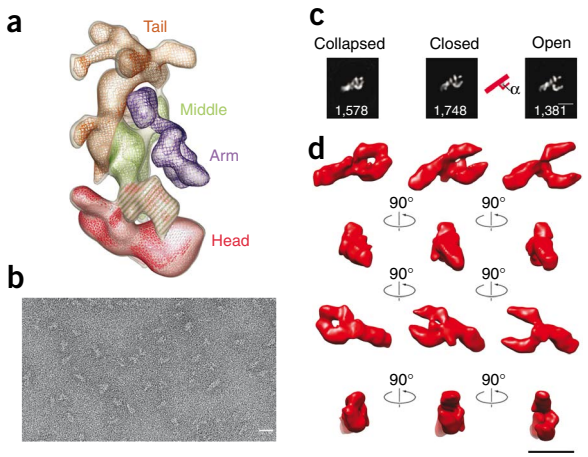

Figure 1 Mediator and Head module structure. (**a**) A cryo-EM reconstruction of Mediator shows the overall structure of the complex at ~25-Å resolution. Previous biochemical, functional and structural analyses suggest a modular organization of Mediator. The Head, Middle/Arm and Tail structural modules have been identified by comparing structures of Mediator in different conformations. A portion of the structurally defined Head module (dashed in green) comprises density corresponding to subunits biochemically identified with the Middle module. (**b**) A micrograph showing single Head module particles preserved in uranyl acetate. Scale bar, 200 Å. (**c**) Three different conformations of the Head module were identified through reference-free alignment and classification of EM images. Head module particles were nearly evenly distributed among the three different conformations that differ in the position of a smaller corner-shaped domain on the bottom-right of the structure. The angle (α) between the larger and smaller portions of the Head module structure (see diagram) is <90° in the collapsed conformation, ~90° in the closed conformation and >90° in the open conformation. Information from images of tilted particles was used to obtain 3D reconstruction of the Head module in all three different conformations. Scale bar, 100 Å. (**d**) Different views of Head module volumes in the collapsed (left column), closed (middle column) and open (right column) conformations. Scale bar, 100 Å.

recombinant protein assemblies by cell breakage followed by affinity purification on a nickel resin through a decahistidine (10×His) tag on the Med17 subunit, and we characterized the assemblies by SDS-PAGE and Coomassie blue staining (**Supplementary Fig. 1**). Expression levels with the MultiBac system were comparable to those obtained with the previous system (data not shown).

Structure and variable conformation of the Head module

We imaged recombinant Head module particles in the electron microscope after preservation in stain. The particles seemed well preserved and similar in size and overall shape (**Fig. 1b**). Reference-free alignment and averaging of Head particle images generated two-dimensional (2D) maps resembling those previously reported[11]. Image classification revealed structural variability resulting from large changes in the position of an extended domain at the distal end (opposite its connection to the rest of Mediator) of the Head structure. Particles adopted three distinct conformations that differed in the angle α at which the movable domain attached to the rest of the structure (collapsed, $\alpha < 90°$; closed, $\alpha \sim 90°$; open, $\alpha > 90°$) (**Fig. 1c**). The collapsed and closed conformations were predominant and accounted for a majority of particles, with only ~30% of particles adopting the open conformation. We obtained three-dimensional (3D) structures of each Head module conformation (at 30- to 35-Å resolution; **Fig. 1d**, **Supplementary Fig. 2**) from images of tilted stained particles using the random conical tilt (RCT) method[13]. The Head portion of a recently published cryo-EM reconstruction of the Mediator complex[8] most closely resembles the closed conformation of the Head, and the comparison suggests that the Head module also adopts different conformations in cryopreserved intact Mediator particles. We attempted cryo-EM analysis, but the combination of conformational flexibility and relatively small size (MW ~230 kDa) make the Head module a very challenging target for such analysis.

EM analysis of Core and Mini Head module subcomplexes

Images of Core particles (missing subunits Med18 and Med20) preserved in stain generated several different 2D averages corresponding to different orientations of Core particles in the EM samples (**Supplementary Fig. 3a**). In all of these averages, the movable portion of the Head module structure was entirely absent (**Fig. 2a**). Consistent with this result, EM analysis of a Head module missing only the Med20 subunit (ΔMed20) resulted in 2D averages in which the tip of the extended movable domain was missing (data not shown), implying that Med18 forms the connection to the rest of the Head structure. We further validated the localization of Med18–Med20 to the movable portion of the Head module structure by difference mapping, a technique in which EM maps of a complex and a related stable subcomplex are compared to obtain direct and accurate subunit localization information[14]. A 2D class average of the Core could be matched to the corresponding portion of a 2D average obtained from images of Head module particles in the collapsed conformation, and difference mapping conclusively identified density corresponding to Med18–Med20 (**Fig. 2a**). Finally, we fitted the X-ray crystal structure of the Med18–Med20 complex[15] (PDB 2HZM) into the variable portion of the 3D EM structure of the Head module and found that it corresponded in size and shape (**Supplementary Fig. 3b**). The peripheral position of the Med18 and Med20 subunits is consistent with biochemical observations regarding Head module subunit interactions[11,16], and their mobility must be at least partially related to reported interaction with the C-terminal portion of Med8, which is in turn connected to a globular Med8 N-terminal domain through an extended linker[15].

Further information about the arrangement of Head module subunits came from class averages calculated from images of the Mini complex (Med11, Med17 and Med22). Comparison of 2D maps of the Mini and Core complexes and difference mapping indicated that subunits Med6 and Med8 form the proximal end (connected to the rest of the Mediator complex) of the Head module structure (**Fig. 2a**). The boundaries between subunits in the Core complex and Med18–Med20, and between subunits in the Mini complex and Med6–Med8, can be delineated by comparing contour plots of the Head, Core and Mini 2D maps (**Fig. 2b**, left). Orienting the 3D reconstruction of the Head module to generate views that approximately correspond to the views in the Head and Core 2D maps (**Fig. 2b**, surface representations in right column) reveals that the views represented by these 2D maps arise from roughly perpendicular orientations of the Head and Core particles in the EM samples (slight differences between the 2D and 3D maps are due to deformation in the 3D reconstructions resulting from some stain-induced specimen deformation and limitations in particle imaging).

To obtain further information about the organization of Med17, the largest Head module subunit to which additional subunits are anchored[11], we analyzed EM images of a mutant recombinant Head

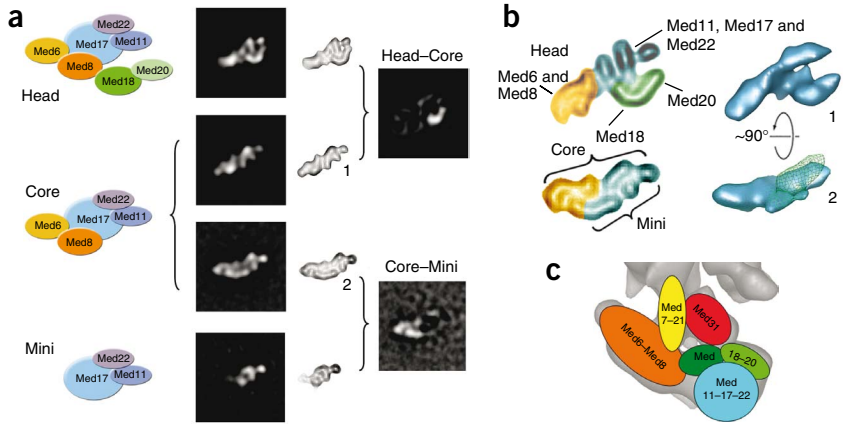

Figure 2 EM analysis of Head module and subcomplexes. (**a**) Comparison of class averages obtained from images of Head and Core subcomplexes (corresponding to approximately the same projection direction) and difference mapping establishes that the extended domain flexibly attached to the rest of the Head module corresponds to subunits Med18 and Med20, with Med18 directly connected to the rest of the Head module structure and Med20 forming the distal end of the mobile domain. The above-mentioned comparison also indicates that the Mini complex corresponds to the left portion of the Core complex structure. All class averages are also shown as contour plots to facilitate visual comparison. (**b**) Contour plots calculated from 2D class averages of the Head and Core complexes were color-coded to highlight the approximate boundaries between different sets of Head module subunits. Two views (marked 1 and 2) of the 3D Head module structure matching the two projections of the Core (also marked 1 and 2) used for difference mapping indicate that the two 2D maps arise from roughly perpendicular orientations of the Head and Core particles in the EM samples (the Med18–Med20 portion of the Head structure is shown as a green mesh in orientation 2). (**c**) The EM results can be used to derive a description of the overall organization of subunits in the Head module and its interface to the rest of the Mediator complex (see **Supplementary Fig. 4** for docking of Med7–Med21 and Med31 into the Mediator cryo-EM structure).

module with an ~200-residue Med17 N-terminal truncation and of an antibody-labeled mutant recombinant Head module with an engineered Med17 N-terminal 10×His tag. We did not unequivocally detect either loss of density in the truncation mutant when compared with the wild-type Head module or antibody density in the tagged mutant, indicating that, in agreement with predictions based on sequence analysis[17], the N-terminal portion of Med17 is poorly ordered.

Considering the 3D reconstructions of the Head module and the 2D maps of the Head, Core and Mini complexes provides an overall description of the subunit organization of the Head module. The Head structure is reminiscent of a wrench in which the handle is formed by subunits Med6 and Med8, the fixed jaw is formed by the Med11, Med17 and Med22 subunits, and the movable jaw is formed by Med18–Med20 (**Fig. 2b**). More detailed information about the location and structure of individual subunits will require X-ray crystallography analysis of the Head module.[ob/ob]

Subunits at the Head–Middle module interface

EM localization of Med6–Med8 and information about Mediator subunit interactions from biochemical studies makes possible the docking of the published X-ray structures of Mediator subunit complexes Med7–Med21 (ref. 18) and Med7(N terminus)–Med31 (ref. 19) into a previous 3D cryo-EM structure of Mediator[8]. The Med7–Med21 heterodimer is part of the Mediator Middle module but has been shown to interact strongly with Head module subunit Med6 (ref. 18). The very elongated shape of the Med7–Med21 complex and the localization of Med6 to the proximal end of the Head module define a unique docking position for the Med7–Med21 X-ray structure in the Mediator cryo-EM volume, and similar considerations define the position of the Med7(N terminus)–Med31 complex (**Supplementary Fig. 4**). In summary, our results allow mapping of the approximate position of Head module subunits and of subunits forming the Head–Middle module interface (**Fig. 2c**).

Interaction with TBP and its effect on Head conformation

Reported interaction between the Med8 N terminus and TBP[15] prompted us to test for TBP binding to the Head, Core and Mini complexes and to investigate the effect of TBP on Head module structure and function. First, we tested physical interaction with TBP in a pulldown assay in which we immobilized GST-tagged Head, Core and Mini complexes on a glutathione-agarose resin and mixed them with recombinant TBP. We probed GST-pulldown fractions for TBP binding by immunoblotting. TBP bound to the immobilized Head module (**Fig. 3a**, lane 4) but not to immobilized GST (**Fig. 3a**, lane 2) or glutathione-agarose resin alone (**Fig. 3a**, lane 1). The Core subcomplex also showed robust (albeit diminished at ~70%) interaction with TBP (**Fig. 3a**, lane 6), whereas the Mini subcomplex showed a diminished (50%) interaction with TBP (**Fig. 3a**, lane 8). We did not observe nonspecific cross-reactivity for any of the Head assemblies (**Fig. 3a**, lanes 3, 5 and 7). These results are consistent with the EM observation of direct Head–TBP interaction and with the idea that multiple Head module subunits contribute to the interaction with TBP. Finally, an *in vitro*–reconstituted transcription assay with highly purified factors used to measure basal transcription activity as a function of TBP concentration in the presence or absence of the Head module revealed that the Head module has a marked effect on transcription levels, which increased two- to three-fold depending on the TBP concentration (**Supplementary Fig. 5**), again consistent with the EM observation of Head–TBP interaction.

To investigate the effect of TBP on the structure of the Head module, we reference-free aligned and classified images of Head module particles incubated with a four-fold molar excess of TBP using hierarchical ascendant clustering[14] into the minimal number of classes (14 total) required to obtain clean class averages (**Fig. 3b**, top row). To quantify the effect of TBP interaction on Head module conformation, and to control for the possibility that conformational changes might have resulted simply from a slightly different orientation of particles on the EM grids or from better image alignment and classification, we matched images of Head module alone to Head–TBP class averages and then reference-free aligned them within each resulting class. This finer classification of Head module images showed that incubation with TBP did not change the orientation of particles in the EM samples or the range of conformations adopted by the Head module (**Fig. 3b**, bottom row). However, incubation with TBP caused ~15% of Head module particles to shift toward the open conformation (**Fig. 3c**).

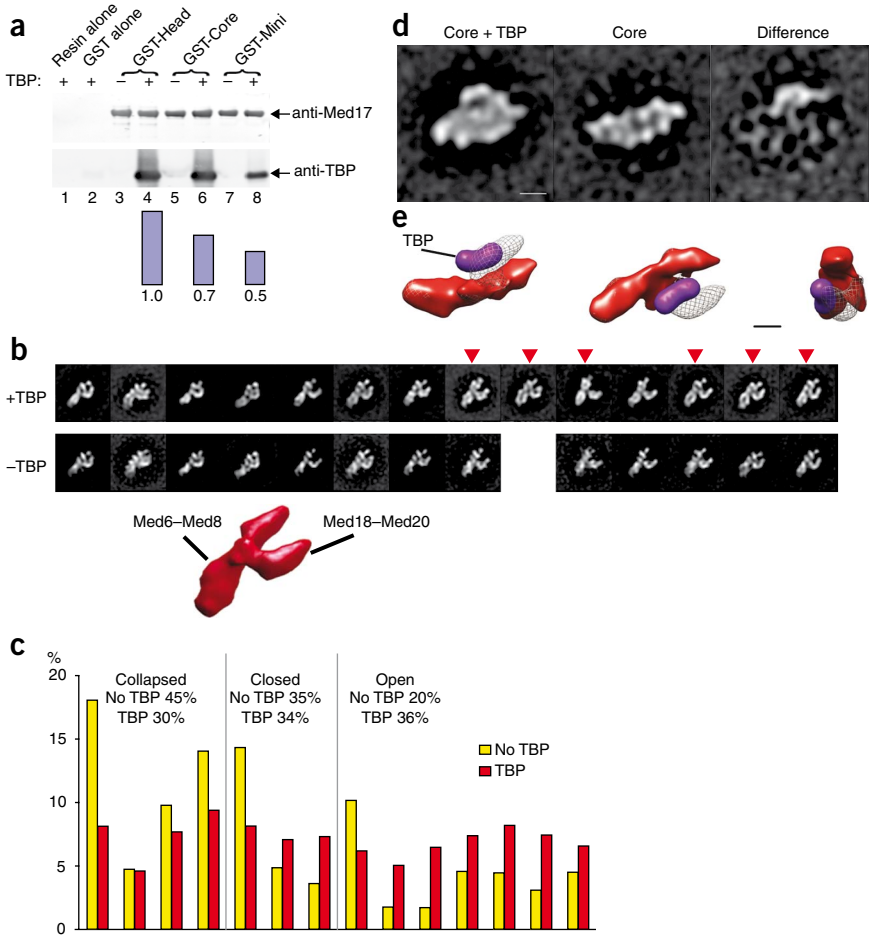

Figure 3 Head–TBP interactions. (**a**) A GST pulldown assay was used to measure the interaction between TBP and the Head, Core and Mini complexes. GST fusion complexes (as indicated) were immobilized on a glutathione-agarose resin incubated in the presence (lanes 4, 6 and 8) or absence (lanes 3, 5 and 7) of TBP. Controls are shown in lanes 1 and 2. Values for relative TBP binding to the different complexes are represented by the bars below the immunoblot. (**b**) Class averages obtained after incubation of the Head module with (top) and without TBP (bottom). Interaction with TBP had no effect on the range of conformations adopted by the Head module. (**c**) TBP interaction influences the distribution of particles among the different conformations of the Head module. The order of groups in the histogram is derived from the order of class averages in **b**. (**d**) Class averages calculated from images of Core particles alone (middle) and after incubation with TBP (left), and the difference between them (right). (**e**) An approximate 3D model of the Head–TBP complex based on the Core + TBP 2D class average and the 3D structure of the Head module. The Core portion of the Head module is shown in red, density corresponding to subunits Med18 and Med20 is represented as a gray mesh, and TBP is shown as a purple surface calculated by low-pass filtering the X-ray structure of TBP[33].

Despite clear evidence for TBP binding and an effect of TBP on Head structure, TBP density could not be conclusively identified in Head–TBP 2D class averages. To further investigate this issue, we incubated TBP with the Core complex, which showed a different orientation on EM samples that might facilitate detection of TBP density. Indeed, a class average including ~10% of images in the Core–TBP data set clearly showed additional density corresponding in size and shape to TBP (**Fig. 3d**). Limited binding of TBP to the Head module in the EM experiments likely resulted from the need to use a comparatively low protein concentration (~50 nM instead of the ~2.6 μM used for the pulldown assays) to obtain a particle density adequate for EM image analysis. TBP binds to the Core across the interface between Mini (Med11, Med17 and Med22) and other Core subunits (Med6 and Med8) and near the Med18 attachment point to the Core (**Fig. 3e**). This is consistent with previously reported binding of TBP to subunit Med8 (ref. 15) and with the results from pulldown analysis indicating comparable binding of TBP to the Head and Core and reduced binding to the Mini complex. Failure to detect distinct TBP density in what we assume must be a similarly small fraction of Head–TBP particle images (only ~15% of Head module particles change conformation after incubation with TBP) is most likely explained by the observation that TBP density would overlap with Core and Med18–Med20 densities in the orientation adopted by Head particles on the EM grids (see **Fig. 2b**).

Interaction of the Head module with Rpb4–Rpb7

A recent model of the Mediator–RNAPII holoenzyme complex structure suggests that the distal end of the Head module interacts closely with the Rpb4–Rpb7 subunit heterodimer[8]. We investigated this by biochemical, genetic and EM analysis. First, we tested direct physical interaction between the Head module and Rpb4–Rpb7 in a pulldown assay in which we immobilized GST-tagged Head module or Head module subassemblies on a glutathione-agarose resin and mixed them with recombinant Rpb4–Rpb7. We probed GST-pulldown fractions for Rpb4–Rpb7 binding by immunoblotting. Rpb4–Rpb7 bound to the immobilized Head module (**Fig. 4a**, lane 4) but not to immobilized GST (**Fig. 4a**, lane 2) or glutathione-agarose resin alone (**Fig. 4b**, lane 1). The Core subcomplex also showed an appreciable (albeit markedly diminished at ~57%) interaction with Rpb4–Rpb7 (**Fig. 4a**, lane 6), whereas the Mini subcomplex only showed a residual (17%) interaction with Rpb4–Rpb7 (**Fig. 4a**, lane 8). We did not observe nonspecific cross-reactivity for any of the Head assemblies (**Fig. 4a**, lanes 3, 5 and 7). These results are consistent with a direct physical interaction between Rpb4–Rpb7 and different Head module subunits, notably Med18 and Med20.

Second, we examined the interaction of the Head module with Rpb4–Rpb7 by EM. We imaged Head module particles after incubation with purified recombinant Rpb4–Rpb7 subunit complex. Additional density was apparent between the jaws of the Head module in a class average obtained from Head module particles in the closed conformation and in a 3D reconstruction obtained using the RCT method on corresponding tilted particle images (**Fig. 4b**). It has been reported that recombinant Med18–Med20 and Rpb4–Rpb7 assemblies do not show a stable interaction[15]. Our biochemical and EM observations suggest that additional Head subunits might be required to stabilize interaction of the Head module with Rpb4–Rpb7.

Finally, we investigated the *in vivo* relevance of the interaction between Rpb4–Rpb7 and Med18–Med20 by assessing the viability of *RPB4* and *MED18* or *MED20* synthetic double mutants. We derived

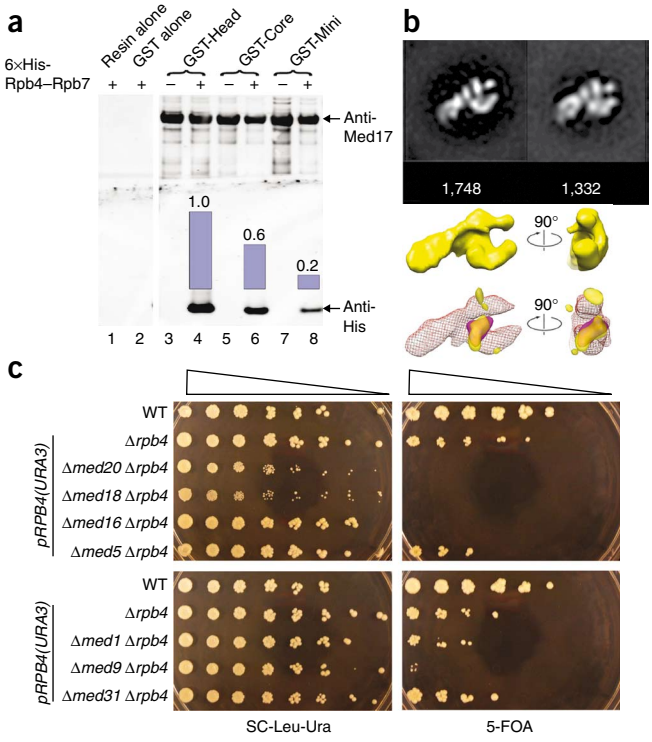

Figure 4 Head module–Rpb4–Rpb7 interaction. (**a**) A GST pulldown assay was used to measure the interactions between Rpb4–Rpb7 and the Head, Core and Mini complexes. GST fusion complexes (as indicated) were immobilized on glutathione-agarose resin incubated in the presence (lanes 4, 6 and 8) or absence (lanes 3, 5 and 7) of recombinant 6×His–Rpb4–Rpb7. Controls are shown in lanes 1 and 2. Values for relative binding to the different complexes are represented by the bars below the immunoblot. (**b**) Comparison of class averages obtained after alignment of Head alone (left, 1,748 images) and Head–Rpb4–Rpb7 particles (right, 1,332 images) shows the presence of additional density in the region corresponding to the jaws of the Head module. A 3D reconstruction of the Head–Rpb4–Rpb7 complex (solid yellow surface, right panel top) shows density (semitransparent yellow surface, right panel bottom) matching the size and shape of a low-resolution model calculated from the Rpb4–Rpb7 X-ray structure[32] (purple surface, right panel bottom). (**c**) Genetic interaction between Rpb4 and Mediator subunits in the Head (Med18 and Med20), Middle (Med1, Med9 and Med31) and Tail (Med16 and Med5) modules was tested by assessing the viability of the synthetic double mutant strains as described in Online Methods. The wild-type (WT) and mutant strains were grown in SC –Leu medium, spotted in five-fold dilutions onto SC –Ura-Leu and SC +5-FOA plates and incubated at 30 °C for 3 (SC –Ura-Leu plates) or 5 d (SC +5-FOA plates).

S. cerevisiae med18 and *med20* deletion strains (*Δmed18* and *Δmed20*, respectively) by replacing the *MED18* or *MED20* gene locus with a *LEU2* marker in a wild-type strain in which a *URA3* marker containing a plasmid-borne *RBP4* gene rescued a chromosomal *RPB4* gene deletion. The *Δmed18* and *Δmed20* mutant strains grew slightly more slowly than the isogenic wild-type strain in synthetic complete medium lacking leucine and uracil (SC –Leu–Ura), but loss of the *RPB4* gene–containing vector upon exposure to 5-fluoroorotic acid (5-FOA) resulted in synthetic lethality, indicating a strong genetic interaction between *RPB4* and *MED18* and/or *MED20* (**Fig. 4c**). To control for the possibility that simultaneous deletion of Rpb4 and any nonessential Mediator subunit might lead to lethality, we carried out analogous double knockout experiments involving nonessential Mediator subunits in the Middle (Med1, Med9 and Med31) and Tail (Med5 and Med15) modules. Simultaneous deletion of Rpb4 and some Mediator subunits in the Middle (Med1 and Med31) and Tail (Med5) modules did not result in lethality, but deletion of Rpb4 and Med9 (Middle) or Med16 (Tail) was lethal (**Fig. 4c**). These results indicate that lethality in these synthetic double mutants is subunit-specific and not a general phenomenon.

The biochemical and genetic analyses of the interaction between Med18–Med20 and Rpb4–Rpb7 are consistent with the direct physical interaction detected by EM analysis and suggest that these proteins underpin a critical Mediator–RNAPII contact. Although we cannot offer direct evidence to explain the Med9-Rpb4 and Med16-Rpb4 genetic interactions, it is interesting to consider that the Middle and Tail modules are also involved in mediating important contacts with RNAPII[8]. It is conceivable that simultaneous deletion of Rpb4 and Med9 or Med16 prevents formation of a stable holoenzyme complex by compromising too many essential Mediator–RNAPII contacts.

DISCUSSION

Subunit organization of the Head module

Single-particle EM analysis reveals that the Head module is organized around a relatively compact core comprising subunits Med17, Med11 and Med22, which form the middle and distal (opposite its connection to the rest of the Mediator structure) portions of the Head module structure (**Fig. 2b**,**c**). Subunits Med6 and Med8 form the proximal end of the Head module structure. The location of the highly conserved Med6 subunit indicates that it is involved in connecting the Head and Middle modules through contacts with Middle module subunits Med7, Med21 and Med31, whose X-ray structures could be docked into the cryo-EM reconstruction of Mediator (**Supplementary Fig. 4**). The interface between the Head and Middle modules is likely important in facilitating a reorganization of the Mediator structure that results in a conformation competent for interaction with RNAPII[8]. Interestingly, a similar conformational change in human Mediator takes place upon binding of a nuclear receptor in an area corresponding to the location of the Med7–Med21–Med31 subunit complex[20].

At the distal end of the Head module, the Med18–Med20 subunit heterodimer forms an extended structure that attaches near the intersection between the Med6–Med8 and Med17–Med11–Med22 subassemblies. Changes in the position of Med18–Med20 result in different overall conformations of the Head module. The EM results presented here provide a description of the subunit organization of the Head module and its connection to the rest of the Mediator complex (**Fig. 2c**).

Head module conformation and its modulation by TBP

Biochemical and EM studies provided evidence for physical interaction between TBP and various subunits in the Head module, with results from pulldown analysis suggesting formation of a nearly stoichiometric Head–TBP complex (**Fig. 3a**). Furthermore, *in vitro* transcription assay results revealed that the Head module causes a marked increase in transcriptional activity at a given TBP concentration (**Supplementary Fig. 5**). The combined effect of the Head module and TBP on basal transcription might be correlated with the effect of TBP on Head module conformation. In the absence of additional factors, the Head module tends to favor conformations in which the movable jaw formed by the Med18 and Med20 subunits is relatively closed (**Fig. 3c**), perhaps due to a reported[15] weak interaction between the Med20 subunit at the distal end of Med18–Med20

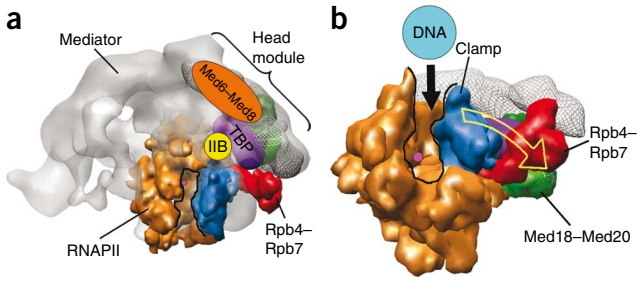

Figure 5 Interaction of the Head module with components of the mPIC and a possible mechanism for initiation regulation. (**a**) Positioning TBP (shown as a purple surface calculated by low-pass filtering the X-ray structure of TBP) in its approximate binding location to the Head module (adjacent to the Med8 subunit) places the transcription factor in a position matching that predicted by current models of the minimal pre-initiation complex structure. This positioning suggests how interaction of RNAPII (shown in orange) with Mediator in the Mediator–RNAPII holoenzyme structure (shown in gray) might help stabilize the pre-initiation complex. The magenta circle denotes the approximate position of the RNAPII active site. (**b**) Interaction of the Head module with the Rpb4–Rpb7 polymerase subunit complex (shown in ruby) documented in this study could be important for enabling Mediator and the general transcription factors to affect the conformation of the polymerase clamp domain (shown in blue), possibly facilitating opening (as indicated by the yellow arrow) of the RNA polymerase II active-site cleft (outlined in black) to allow access of double-stranded promoter DNA to the polymerase active site.

subassembly and the Med17 subunit in the opposite jaw (**Fig. 2b**). However, after incubation with TBP, the open conformation of the Head module becomes prevalent (**Fig. 3c**). We do not have any information about the mechanism that enables TBP to affect Head module conformation, but our observations suggest that a shift to the open conformation of the Head module jaws upon interaction with TBP could be important for Mediator interaction with RNAPII.

Head module interaction with RNAPII

The possible implications of Head module interaction with RNAPII can be better appreciated by considering the structure of the Mediator–RNAPII holoenzyme. Fitting the 3D Head module reconstruction described here and the atomic-resolution structure of the 12-subunit initiation-competent form of RNAPII[21,22] into the Mediator–RNAPII holoenzyme structure[8,23] suggests how Mediator establishes a critical contact with RNAPII and how Mediator might stabilize the PIC and influence transcriptional initiation.

The approximate position of TBP in the Mediator–RNAPII holoenzyme structure can be deduced from the location of TBP binding to the recombinant Head Core assembly (**Fig. 3d**,**e**). Based on this result, in the holoenzyme complex, TBP would be located at the back of the RNAPII, near the dock domain[24] where, in agreement with current models for the organization of a minimal PIC[24–26], it would be positioned to interact with TFIIB and upstream promoter DNA. This arrangement could help explain the observed stabilization of the PIC by Mediator (**Fig. 5a**).

The structure of the Mediator–RNAPII holoenzyme indicates that Rpb4–Rpb7 constitutes a major contact between the Mediator Head module and RNAPII[8]. Accordingly, we have documented a strong genetic and physical interaction between recombinant Head module and recombinant Rpb4–Rpb7 (**Fig. 4**). The Rpb4–Rpb7 complex binds between the jaws of the Head module, which adopt an open conformation to accommodate Rpb4–Rpb7 binding. This brings up the possibility that regulation of Head conformation by factors such as TBP could directly influence interaction of Mediator with RNAPII.

Implications of the interaction between Head and Rpb4–Rpb7

Polymerase subunits Rpb4 and Rpb7 appear to be involved in a number of events, from nascent RNA binding[27] to the stress response and recruitment of CTD-interacting complexes[28]. Notably, the subunits are essential for promoter-dependent initiation but not for elongation[29], and they appear to be involved in a step of initiation subsequent to recruitment of RNAPII to the PIC[30]. Recent analysis suggests that physical interaction with RNAPII underlies the essential role of Rpb7 in the cell[31]. The results presented here suggest that this might at least in part be due to the critical role Rpb4 and Rpb7 play in enabling interaction of Mediator with RNAPII.

Conceivably, Rpb4–Rpb7 could act as more than an attachment point for the Head module, perhaps helping Mediator modulate access of promoter DNA to the RNAPII cleft. It has been suggested[21,22] that interaction of the N terminus of Rpb7 with the switch domains at the base of the RNAPII clamp would prevent the latter from adopting a more open conformation that would be necessary to accommodate double-stranded DNA in the RNAPII active site cleft. Rather than blocking clamp movement, the interaction of Rpb4 and Rpb7 (the N terminus of Rpb4 also interacts with the clamp[31,32]) with the clamp might allow the subunits to function as a 'handle' that could facilitate clamp movement in response to interaction of RNAPII with Mediator and other components of the transcription machinery (**Fig. 5b**). Further analysis of RNAPII clamp mobility and the way in which it is affected by basal transcription factors and the Head module will be necessary to test this hypothesis.

METHODS

Methods and any associated references are available in the online version of the paper at http://www.nature.com/nsmb/.

Note: Supplementary information is available on the Nature Structural & Molecular Biology website.

ACKNOWLEDGMENTS

We thank I. Berger (European Molecular Biology Laboratory France) for providing reagents and help to establish the MultiBac expression system and C. Kaplan (Texas A&M Univ.), G. Hartzog (Univ. of California, Santa Cruz) and M. Goebl (Indiana Univ.) for providing yeast vectors and advising on the implementation of genetic experiments. This work was supported by US National Institutes of Health grant R01 GM67167 (F.J.A.) and US National Science Foundation grant MCB 0843026 (Y.T.), an American Heart Association Scientist Development Award 0735395N (Y.T.) and a Human Frontier Science Program long-term fellowship (T.I.).

AUTHOR CONTRIBUTIONS

T.I., F.C. and Y.T. expressed, purified and biochemically characterized recombinant Head module and Head module subcomplexes and provided recombinant Rpb4 and Rpb7 and TBP; Y.T. and T.I. designed and carried out Head–Rpb4–Rpb7 and Head–TBP binding assays; K.Y. and Y.T. designed and carried out assays to test genetic interaction of Mediator subunits with Rpb4; Y.T. carried out *in vitro* transcription assays; G.C. carried out all EM data collection and analysis; G.C., Y.T. and F.J.A. discussed and interpreted all results; F.J.A. supervised EM structural analysis and wrote the manuscript in collaboration with G.C. and Y.T.

COMPETING INTERESTS STATEMENT

The authors declare no competing financial interests.

Published online at http://www.nature.com/nsmb/.
Reprints and permissions information is available online at http://npg.nature.com/reprintsandpermissions/.

1. Flanagan, P.M. *et al.* Resolution of factors required for the initiation of transcription by yeast RNA polymerase II. *J. Biol. Chem.* **265**, 11105–11107 (1990).
2. Flanagan, P.M., Kelleher, R.J. III., Sayre, M.H., Tschochner, H. & Kornberg, R.D. A mediator required for activation of RNA polymerase II transcription *in vitro*. *Nature* **350**, 436–438 (1991).
3. Baek, H.J., Malik, S., Qin, J. & Roeder, R.G. Requirement of TRAP/mediator for both activator-independent and activator-dependent transcription in conjunction with TFIID-associated TAF(II)s. *Mol. Cell. Biol.* **22**, 2842–2852 (2002).
4. Naar, A.M. *et al.* Composite co-activator ARC mediates chromatin-directed transcriptional activation. *Nature* **398**, 828–832 (1999).
5. Takagi, Y. & Kornberg, R.D. Mediator as a general transcription factor. *J. Biol. Chem.* **281**, 80–89 (2006).
6. Asturias, F.J., Jiang, Y.W., Myers, L.C., Gustafsson, C.M. & Kornberg, R.D. Conserved structures of mediator and RNA polymerase II holoenzyme. *Science* **283**, 985–987 (1999).
7. Sato, S. *et al.* A set of consensus mammalian mediator subunits identified by multidimensional protein identification technology. *Mol. Cell* **14**, 685–691 (2004).
8. Cai, G., Imasaki, T., Takagi, Y. & Asturias, F.J. Mediator structural conservation and implications for the regulation mechanism. *Structure* **17**, 559–567 (2009).
9. Holstege, F.C. *et al.* Dissecting the regulatory circuitry of a eukaryotic genome. *Cell* **95**, 717–728 (1998).
10. Thompson, C.M. & Young, R.A. General requirement for RNA polymerase II holoenzymes *in vivo*. *Proc. Natl. Acad. Sci. USA* **92**, 4587–4590 (1995).
11. Takagi, Y. *et al.* Head module control of mediator interactions. *Mol. Cell* **23**, 355–364 (2006).
12. Fitzgerald, D.J. *et al.* Protein complex expression by using multigene baculoviral vectors. *Nat. Methods* **3**, 1021–1032 (2006).
13. Radermacher, M. The three-dimensional reconstruction of single particles from random and non-random tilt series. *J. Electron Microsc. Tech.* **9**, 359–394 (1988).
14. Frank, J. *Three-Dimensional Electron Microscopy of Macromolecular Assemblies* 410 (Oxford University Press, San Diego, California, USA, 2006).
15. Lariviere, L. *et al.* Structure and TBP binding of the Mediator head subcomplex Med8-Med18-Med20. *Nat. Struct. Mol. Biol.* **13**, 895–901 (2006).
16. Koh, S.S., Ansari, A.Z., Ptashne, M. & Young, R.A. An activator target in the RNA polymerase II holoenzyme. *Mol. Cell* **1**, 895–904 (1998).
17. Toth-Petroczy, A. *et al.* Malleable machines in transcription regulation: the mediator complex. *PLOS Comput. Biol.* **4**, e1000243 (2008).
18. Baumli, S., Hoeppner, S. & Cramer, P. A conserved mediator hinge revealed in the structure of the MED7.MED21 (Med7.Srb7) heterodimer. *J. Biol. Chem.* **280**, 18171–18178 (2005).
19. Koschubs, T. *et al.* Identification, structure, and functional requirement of the Mediator submodule Med7N/31. *EMBO J.* **28**, 69–80 (2009).
20. Taatjes, D.J., Schneider-Poetsch, T. & Tjian, R. Distinct conformational states of nuclear receptor-bound CRSP-Med complexes. *Nat. Struct. Mol. Biol.* **11**, 664–671 (2004).
21. Bushnell, D.A. & Kornberg, R.D. Complete, 12-subunit RNA polymerase II at 4.1-Å resolution: implications for the initiation of transcription. *Proc. Natl. Acad. Sci. USA* **100**, 6969–6973 (2003).
22. Armache, K.J., Kettenberger, H. & Cramer, P. Architecture of initiation-competent 12-subunit RNA polymerase II. *Proc. Natl. Acad. Sci. USA* **100**, 6964–6968 (2003).
23. Davis, J.A., Takagi, Y., Kornberg, R.D. & Asturias, F.A. Structure of the yeast RNA polymerase II holoenzyme: Mediator conformation and polymerase interaction. *Mol. Cell* **10**, 409–415 (2002).
24. Bushnell, D.A., Westover, K.D., Davis, R.E. & Kornberg, R.D. Structural basis of transcription: an RNA polymerase II-TFIIB cocrystal at 4.5 Angstroms. *Science* **303**, 983–988 (2004).
25. Chung, W.H. *et al.* RNA polymerase II/TFIIF structure and conserved organization of the initiation complex. *Mol. Cell* **12**, 1003–1013 (2003).
26. Chen, H.T. & Hahn, S. Mapping the location of TFIIB within the RNA polymerase II transcription preinitiation complex: a model for the structure of the PIC. *Cell* **119**, 169–180 (2004).
27. Todone, F., Brick, P., Werner, F., Weinzierl, R.O. & Onesti, S. Structure of an archaeal homolog of the eukaryotic RNA polymerase II RPB4/RPB7 complex. *Mol. Cell* **8**, 1137–1143 (2001).
28. Sampath, V. & Sadhale, P. Rpb4 and Rpb7: a sub-complex integral to multi-subunit RNA polymerases performs a multitude of functions. *IUBMB Life* **57**, 93–102 (2005).
29. Edwards, A.M., Kane, C.M., Young, R.A. & Kornberg, R.D. Two dissociable subunits of yeast RNA polymerase II stimulate the initiation of transcription at a promoter *in vitro*. *J. Biol. Chem.* **266**, 71–75 (1991).
30. Orlicky, S.M., Tran, P.T., Sayre, M.H. & Edwards, A.M. Dissociable Rpb4-Rpb7 subassembly of rna polymerase II binds to single-strand nucleic acid and mediates a post-recruitment step in transcription initiation. *J. Biol. Chem.* **276**, 10097–10102 (2001).
31. Sampath, V., Balakrishnan, B., Verma-Gaur, J., Onesti, S. & Sadhale, P.P. Unstructured N terminus of the RNA polymerase II subunit Rpb4 contributes to the interaction of Rpb4.Rpb7 subcomplex with the core RNA polymerase II of *Saccharomyces cerevisiae*. *J. Biol. Chem.* **283**, 3923–3931 (2008).
32. Armache, K.J., Mitterweger, S., Meinhart, A. & Cramer, P. Structures of complete RNA polymerase II and its subcomplex, Rpb4/7. *J. Biol. Chem.* **280**, 7131–7134 (2005).
33. Kim, Y., Geiger, J.H., Hahn, S. & Sigler, P.B. Crystal structure of a yeast TBP/TATA-box complex. *Nature* **365**, 512–520 (1993).

ONLINE METHODS

Expression and purification of Head module and subcomplexes. We expressed Head module and its subcomplexes in insect cells using the MultiBac system[12]. We amplified open reading frames (ORFs) of genes encoding 10×His-Med17, Med6, Med18, Med8, Med19, Med20, Med22 and Med11 by PCR from pBacPAK9 vectors as described previously[11]. We cloned the ORFs into SphI and SmaI sites (MCS1) and BamHI and HindIII sites (MCS2) of the pFL vector using the sequence- and ligation-independent cloning method[34], resulting in vectors pFL-Med22–Med11, pFL-Med6–Med8, pFL-Med18–Med20 and pFL–10×His-Med17. We performed cloning of a PmeI and AvrII fragment from one vector into SpeI and NruI sites of another as described[12], yielding vectors pFL-Med22–10×His-Med17–Med11 (pYT67) for the Mini complex[11], pUCDM-Med6–Med8 (pYT110), pUCDM-Med22–Med11 (pYT111) and pSPL-Med18–Med20 (pYT75). Fusion of the pYT67 and pYT110 vectors yielded the vector for the Core complex. Fusion of the pYT67, pYT110 and pYT75 vectors yielded the vector for the 10×His-tagged full Head module.

We constructed vector pFL–10×GST-Med17 (pYT605) by introducing a GST tag (amplified from the pGEX6P-1 vector (GE Health) by PCR) between the 10×His tag and the Med17 ORF of pFL–10×His-Med17. Further subcloning resulted in vectors pUCDM-Med6–Med22–Med11–Med8 (pYT120) and pUCDM-Med6–Med22–Med18–Med20–Med11–Med8 (pYT151). Fusion of the pYT605 vector with pYT111, pYT120 or pYT151 yielded 10×His-GST–tagged versions of the Head, Core and Mini complexes, respectively. We used these transfer vectors to produce high-titer viruses in Sf9 cells as described[12]. We carried out expression and purification of Head module, subcomplexes and 10×His-GST fusion versions as described[11].

EM sample preparation, data collection and image analysis. We diluted purified recombinant Head module and Head module subcomplexes to ~10 μg ml^{-1} (25 mM KCl, 25 mM Tris-HCl (pH 7.8), 5 mM DTT). To characterize the interaction of the Head and Core modules with TBP, we diluted the complexes to a concentration of 100 μg ml^{-1} and mixed them with TBP at a 1:4 Head (or Core) to TBP molar ratio. After incubation on ice for 2 h, we diluted the mixtures to a final Head (or Core) module concentration of ~10 μg ml^{-1} with the same buffer used for dilution of the Head module and its subcomplexes. To characterize the interaction of the Head module with Rpb4–Rpb7, we mixed the two at a 1:5 Head to Rpb4–Rpb7 molar ratio, incubated them overnight (12 h) at 4 °C and diluted them 30-fold (Head module final concentration ~7.5 μg ml^{-1}). We prepared EM samples as described previously[35].

We recorded untilted images of the Head module and subcomplexes as well as of the Head and Core complexes with TBP using a Tecnai Spirit (Philips/FEI) microscope (LaB_6 filament, low-dose conditions, 120-kV accelerating voltage, ~1-μm underfocus). We recorded images with a Tietz (TVIPS GmbH) CCD camera at 42,000× magnification (5.06 Å per pixel). We obtained tilted (55°) and untilted image pairs of Head and Head–Rpb4–Rpb7 particles under low-dose conditions using a Tecnai F20 microscope (Philips/FEI) (field emission gun, low-dose conditions, 120-kV accelerating voltage, ~0.3- to 0.6-μm underfocus). We recorded images on Kodak SO163 film at 50,000× magnification. We three-fold pixel-averaged digitized images (7 μm sampling step size) to 4.2 Å per pixel. We selected Head and Head–Rpb4–Rpb7 particle images from digitized micrograph pairs using the TiltPicker program[36] and montaged them for interactive screening, yielding ~7,000 Head module and ~8000 Head–Rpb4–Rpb7 single-particle tilt-pair images.

We carried out analysis of Head module, Head module subcomplexes and Head–TBP images using the SPIDER software package[37]. We calculated 3D reconstructions of the Head module and the Head–Rpb4–Rpb7 complexes using the random conical tilt method[13]. We initially analyzed Core–TBP and Head–Rpb4–Rpb7 images using the Xmipp package[38]. We then used the resulting averages to run iterative alternating rounds of supervised multireference alignment and classification as well as reference-free alignment with Spider to improve the homogeneity of the image classes[35]. We produced all molecular graphics images using Chimera[39].

Head module–Rpb4–Rpb7 genetic interaction experiments. We amplified a DNA fragment including the *RPB4* locus (1 kb upstream and downstream of ORF) by PCR from yeast genomic DNA and cloned it into the EcoRI and HindIII sites of *pRS316(URA3)*, yielding pYT505 (pRS316-RPB4). We transformed pYT505 into an *rpb4* deletion yeast strain from Open Biosystems (*MATα leu2Δ0*, *lys2Δ0*, *ura3Δ0*, *rpb4*::*Kan*^{r}), resulting in yeast strain YT204. We derived deletion strains from YT204 by replacing the corresponding open reading frames with a PCR-generated *LEU2* cassette. Finally, we introduced empty vectors, pRS415(LEU2) and/or pRS316(URA3) into YT202 and BY4742 (Open Biosystems), yielding YT207 and YT228 (WT). Genotypes of the yeast strains used in this study are described (**Supplementary Table 1**). We grew the wild-type and deletion-mutant yeast strains for 2 d in SC –Leu medium. We then spotted cells in five-fold dilutions onto SC –Ura–Leu and SC +5-FOA plates and incubated them at 30 °C for 3 d for SC –Ura–Leu plates and 5 d for SC +5-FOA plates.

Head–Rpb4/Rpb7 and Head–TBP binding assays. We immobilized ~20 μg of 10×His-GST–tagged Head, Core or Mini complexes or GST (as a control) on 30 μl glutathione-agarose resin in buffer A100 (100 mM potassium acetate, 50 mM HEPES-KOH (pH 7.6), 10% (v/v) glycerol, 5 mM β-mercaptoethanol). We incubated the resin alone or mixed it with ~12 μg recombinant 6×His–Rpb4–Rpb7 (prepared according to ref. 40 and kindly provided by G. Calero) or ~7.2 μg of recombinant TBP at 4 °C for 1 h. The Head:TBP and Head:Rpb4–Rpb7 molar ratios were both ~1:3. After removal of the flow-through, we washed the resin three times with 200 μl buffer A100. We eluted bound proteins by mixing the resin with 30 μl 2× NuPAGE loading buffer. We subjected the eluates to immunoblotting probed for the Head module with anti-Med17 antibody as described[5]. We used anti–His tag antibody (GenScript) to probe for 6×His-Rpb7 and anti-TBP antibody to probe for TBP. We carried out detection using Dylight 680 goat anti–rabbit IgG (Pierce) and scanning with an Odyssey infrared imaging system (LI-COR Biosciences). We carried out the quantification using the Multi-Gauge software package (FUJIFILM Life Science).

34. Li, M.Z. & Elledge, S.J. Harnessing homologous recombination *in vitro* to generate recombinant DNA via SLIC. *Nat. Methods* **4**, 251–256 (2007).
35. Brignole, E.J., Smith, S. & Asturias, F.J. Conformational flexibility of metazoan fatty acid synthase enables catalysis. *Nat. Struct. Mol. Biol.* **16**, 190–197 (2009).
36. Voss, N.R., Yoshioka, C.K., Radermacher, M., Potter, C.S. & Carragher, B. DoG Picker and TiltPicker: software tools to facilitate particle selection in single particle electron microscopy. *J. Struct. Biol.* **166**, 205–213 (2009).
37. Frank, J. *et al.* SPIDER and WEB: processing and visualization of images in 3D electron microscopy and related fields. *J. Struct. Biol.* **116**, 190–199 (1996).
38. Sorzano, C.O. *et al.* XMIPP: a new generation of an open-source image processing package for electron microscopy. *J. Struct. Biol.* **148**, 194–204 (2004).
39. Pettersen, E.F. *et al.* UCSF Chimera-a visualization system for exploratory research and analysis. *J. Comput. Chem.* **25**, 1605–1612 (2004).
40. Sakurai, H., Mitsuzawa, H., Kimura, M. & Ishihama, A. The Rpb4 subunit of fission yeast *Schizosaccharomyces pombe* RNA polymerase II is essential for cell viability and similar in structure to the corresponding subunits of higher eukaryotes. *Mol. Cell. Biol.* **19**, 7511–7518 (1999).

doi:10.1038/nsmb.1757